Low-Complexity ICI Suppression for OFDM Over Time- and Frequency-Selective Rayleigh Fading Channels

Xiaodong Cai and Georgios B. Giannakis
Dept. of ECE, University of Minnesota
200 Union Street SE, Minneapolis, MN 55455
Email:{caixd,georgios}@ece.umn.edu *

Abstract

While rapid variations of the fading channel cause intercarrier interference (ICI) in OFDM, thereby degrading its performance considerably, they also introduce temporal diversity, which can be exploited to improve the performance. In this paper, we first derive a matched filter bound (MFB) for OFDM transmissions over doubly-selective Rayleigh fading channels, which benchmarks the best possible performance if ICI is completely cancelled without noise enhancement. We then develop low-complexity MMSE and DFE receivers for ICI suppression. Simulations show that the DFE receiver can collect significant gains of ICI-impaired OFDM with affordable complexity.

1 Introduction

In a wireless environment, the multipath channel of a user is time-varying because of the user's mobility. Channel variations may also arise due to the presence of an unknown carrier frequency offset (CFO). While subcarriers in OFDM are orthogonal in the presence of the time-invariant multipath channel, the rapid channel variations in a symbol period destroy the orthogonality among subcarriers, which results in intercarrier interference (ICI) [7, 10]. In [1, 12], by mapping symbols to a group of subcarriers, self-cancellation schemes render the OFDM signal less sensitive to the CFO-induced ICI, at the price of sacrificing some bandwidth. Since CFO can be estimated accurately, the CFO-induced ICI can also be canceled efficiently by compensating for CFO at the receiver.

While suppression of the CFO-induced ICI is relatively easy to implement, it is more challenging to cancel the ICI resulted from Doppler spread of the time-varying fading channel. A linear MMSE equalizer and a successive interference cancellation (SIC) scheme with the optimal ordering were advocated in [4]. Since the number of subcarriers N is usually very large, e.g., $N = 1512$ or 6048 in digital video broadcasting (DVB) [11], even the linear MMSE equalizer proposed in [4] demands very high computation, and it may not be practically feasible.

In this paper, we first derive a matched filter bound (MFB) for OFDM over doubly-selective channels. We then show that the most of the symbol energy is distributed on a few subcarriers, and the ICI power on a subcarrier mainly comes from several neighboring subcarriers. Based on this observation, we develop a low-complexity MMSE equalizer for ICI suppression. While the MMSE equalizer still exhibits an error floor on BER, and loses the temporal diversity, a low-complexity decision feedback (DFE) equalizer will be derived to collect the diversity, and bring the overall system performance closer to the MFB.

Notation: Superscripts ^{T}, * and $^{\mathcal{H}}$ stand for transpose, conjugate, Hermitian, respectively; and $z = y \bmod x$ yields the smallest $z \geq 0$ so that $y = nx + z$ for a non-negative integer n. Column vectors (matrices) are denoted by boldface lower (upper) case letters. We will use $\boldsymbol{\mathcal{D}}(\mathbf{x})$ to denote a diagonal matrix with $\mathbf{x}$ on its diagonal, $\mathbf{A}(m,n)$ to denote the (m,n)th entry of the matrix $\mathbf{A}$, $\mathbf{x}(m)$ to denote the mth entry of the vector $\mathbf{x}$. The matrix $\mathbf{F}_N(m,n) := N^{-1/2}\exp(-j2\pi(m-1)(n-1)/N)$ stands for the $N \times N$ discrete Fourier transform (DFT) matrix, and $\mathbf{f}_m$ stands for the mth column of $\mathbf{F}_N$. We will use Matlab notation $\mathbf{A}(m:n,:)$ ($\mathbf{A}(:,m:n)$) to extract row (column) m to row (column) n, $\mathbf{A}(\mathbf{r},\mathbf{c})$ to extract a submatrix within $\mathbf{A}$ defined by the index vector of desired rows in $\mathbf{r}$ and the index vector of desired columns in $\mathbf{c}$, $\mathbf{x}(m:n)$ to extract entry m to entry n, and $\mathbf{x}(\mathbf{r})$ to extract entries by the index vector $\mathbf{r}$.

2 Signal Model and MFB

2.1 Signal Model

Suppose the symbol duration after serial-to-parallel (S/P) conversion is T_s. The entire signal bandwidth is covered by N subcarriers, and the space between two neighboring subcarries is $1/T_s$. Denote the chip duration by $T_c := T_s/N$, and assume that the length of cyclic prefix is N_pT_c with a integer N_p. The duration of an OFDM block is $T_b := (N+N_p)T_c$. The discrete transmitted

*Work in this paper was supported by the ARL/CTA grant no. DAAD19-01-2-011.

signal in a block with cyclic prefix is given by

$$u(n) := u(nT_c) = \frac{1}{\sqrt{N}} \sum_{k=0}^{N-1} s_k e^{j2\pi kn/N}, \qquad (1)$$

where $n \in [-N_p, N-1]$, and s_k is the information bearing symbol on the kth subcarrier. We assume that all symbols have the same energy $E_s = E[\,|s_k|^2\,]$.

Let the impulse response of the time-varying multipath channel be $h(t;\tau) = \sum_{d=0}^{L-1} h(t; lT_c)\delta(\tau - lT_c)$. The autocorrelation function of the channel is given by $E[h(t;\tau_1)h^*(t+\triangle t;\tau_2)] = \phi_h(\triangle t;\tau_1)\delta(\tau_1-\tau_2)$ [9, p.762]. In a rich-scattering environment, the autocorrelation function is separable in time and delay [6]: $\phi_h(\triangle t;\tau) = \phi_t(\triangle t)\phi_\tau(\tau)$, where $\phi_t(\triangle t)$ is the time-correlation function, and $\phi_\tau(\tau)$ is the delay power spectrum [9, p.762]. In the Rayleigh fading channel, $h(t, lT_c)$ is complex Gaussian with zero-mean and variance $\sigma_l^2 := \phi_\tau(lT_c)$, and $\{h(t, lT_c)\}\}_{l=0}^{L-1}$ are independent. The channel is assumed to be normalized, i.e., $\sum_{l=0}^{L-1}\sigma_l^2 = 1$.

We assume that $N_p \geq L$, and hence interblock interference (IBI) is completely eliminated. The discrete received signal without IBI is given by $r(n) = x(n) + w(n)$, $n \in [0, N-1]$, where

$$x(n) = \sum_{l=0}^{L} h_d(n,l)u(n-l),\ n \in [0, N-1], \qquad (2)$$

$h_d(n,l) := h(nT_c, lT_c)$, and $w(n)$ is a complex Gaussian random variable with zero-mean and variance $N_0/2$ per dimension. Let the channel frequency response on the kth subcarrier, at time nT_c, be $H(n,k) := \sum_{l=0}^{L} h_d(n,l)\ \exp(-j2\pi kl/N) = \tilde{\mathbf{f}}_k^T\mathbf{h}(n)$, where $\tilde{\mathbf{f}}_k = \sqrt{N}\,\mathbf{f}_k(1:L+1)$. Let $\mathbf{x} = [x(0),\ldots,x(N-1)]^T$, $\tilde{\mathbf{h}}_k = [H(0,k),\ldots,H(N-1,k)]^T$. Substituting (1) into (2), we obtain $\mathbf{x} = \sum_{k=0}^{N-1}\boldsymbol{\mathcal{D}}(\mathbf{f}_k^*)\tilde{\mathbf{h}}_k s_k$, and the received signal vector $\mathbf{r} = [r(0),\ldots,r(N-1)]^T$ can be written as $\mathbf{r} = \mathbf{x}+\mathbf{w}$, where $\mathbf{w} = [w(0),\ldots,w(N-1)]^T$. To demodulate the symbols on different subcarriers, we perform FFT on $\mathbf{r}$, and obtain $\mathbf{y} = \mathbf{F}_N\mathbf{r} = \tilde{\mathbf{x}} + \tilde{\mathbf{w}}$, where $\tilde{\mathbf{x}} = \mathbf{F}_N\mathbf{x}$, and $\tilde{\mathbf{w}}$ is still white Gaussian noise since $\mathbf{F}_N$ is unitary. Letting $\mathbf{s} := [s_0,\ldots,s_{N-1}]^T$, $\mathbf{A}(m,k) := \mathbf{f}_m^T\boldsymbol{\mathcal{D}}(\mathbf{f}_k^*)\tilde{\mathbf{h}}_k$, we have $\tilde{\mathbf{x}} = \mathbf{A}\mathbf{s}$; and $\mathbf{y}$ becomes

$$\mathbf{y} = \mathbf{A}\mathbf{s} + \tilde{\mathbf{w}}. \qquad (3)$$

Since $\mathbf{f}_m^T\boldsymbol{\mathcal{D}}(\mathbf{f}_k^*)\mathbf{1} = \delta(m-k)$, the matrix $\mathbf{A}$ is diagonal if all entries of $\tilde{\mathbf{h}}_k$ are equal, where $\mathbf{1}$ denotes the vector with all 1 entries. Hence, if the channel is fixed in a block, there is no ICI.

2.2 Matched Filter Bound

To derive an MFB, we suppose that there is only one subcarrier, say subcarrier k, transmitting a symbol s_k. The received block $\mathbf{y}$ in (3) becomes $\mathbf{y} = \mathbf{F}_N\boldsymbol{\mathcal{D}}(\mathbf{f}_k^*)\tilde{\mathbf{h}}_k s_k + \tilde{\mathbf{w}}$. The matched filter output is written as $z = \tilde{\mathbf{h}}_k^{\mathcal{H}}\boldsymbol{\mathcal{D}}(\mathbf{f}_k)\mathbf{F}_N^{\mathcal{H}}\mathbf{y} = N^{-1}\tilde{\mathbf{h}}_k^{\mathcal{H}}\tilde{\mathbf{h}}_k s_k + \nu$, where ν is Gaussian noise with zero-mean and variance $N^{-1}\tilde{\mathbf{h}}_k^{\mathcal{H}}\tilde{\mathbf{h}}_k N_0$. Defining the time-correlation matrix $\boldsymbol{\Phi}_t(m,n) := \phi_t(|m-n|T_c)$, we can write the covariance matrix of $\tilde{\mathbf{h}}_k$ as $\mathbf{R}_{\tilde{h}_k} = E[\tilde{\mathbf{h}}_k\tilde{\mathbf{h}}_k^{\mathcal{H}}] = \boldsymbol{\Phi}_t$. Suppose that the rank of $\boldsymbol{\Phi}_t$ is r, and the r non-zero eigenvalues are λ_i, $i \in [1, r]$. Then, z can be expressed as $z = \sum_{i=1}^{r}\gamma_i|\breve{h}_i|^2 s_k + \nu$, where $\breve{h}_i$, $i \in [1, r]$ are zero-mean complex Gaussian random variables with unit variance, and $\gamma_i = \lambda_i/N$. If all eigenvalues λ_i, $i \in [1, r]$ are distinct, the BER for BPSK and QPSK can be found as [8]

$$P_e = \frac{1}{2}\sum_{i=1}^{r}\mu_i\left[1 - \sqrt{E_b\gamma_i/(E_b\gamma_i + N_0)}\right], \qquad (4)$$

where $\mu_i = \prod_{j=1,\,j\neq i}^{r}\gamma_i/(\gamma_i-\gamma_j)$, $E_b = E_s$ for BPSK, and $E_b = E_s/2$ for QPSK. When some eigenvalues are identical, the BER can also be found as in [8].

Remark 1 If the channel is fixed in a symbol period, entries of $\boldsymbol{\Phi}_t$ are all 1's, thus $r = 1$; but when the channel is rapidly varying, the rank of the Hermitian matrix $\boldsymbol{\Phi}_t$ will be greater than 1, i.e., $r > 1$. Hence, the variations of the channel introduce temporal diversity.

3 ICI Suppression

3.1 ICI and Symbol Energy Leakage

In [2], a universal upper bound on total ICI power P_I caused by continuous Doppler spectrum is found as

$$P_I^{(\mathrm{ub1})} = \frac{E_s\int_0^1[1-\mathrm{sinc}^2(f_dT_sf)]^2dt}{\int_0^1[1-\mathrm{sinc}^2(f_dT_sf)]dt}, \qquad (5)$$

where f_d is the maximum Doppler frequency. If the ICI is caused by an unknown CFO, f_{CFO}, which can be viewed as a random variable in $[0, f_d]$, the upper bound on P_I can be written as

$$P_I^{(\mathrm{ub2})} = \begin{cases} E_s[1-\mathrm{sinc}^2(f_dT_s)], & f_dT_s < 1 \\ E_s, & f_dT_s \geq 1. \end{cases} \qquad (6)$$

These bounds are much tighter than the bound in [7]. Comparing the universal bounds (5) and (6) reveals that for a given maximum Doppler frequency f_d, the largest ICI power is caused by a deterministic carrier frequency offset at $f_{CFO} = f_d$ [2].

Let $P_{I,Q}$ be the ICI power on the kth subcarrier from the subcarriers $k-1$ to $k-Q$ and $k+1$ to $k+Q$, where Q is a positive integer. A universal lower bound on the normalized partial ICI $P_{I,Q}$ is given by [2]

$$P_{I,Q}/P_I \geq \vartheta/(1+\vartheta), \qquad (7)$$

where $\vartheta = 2S(Q)/[\pi^2/3 - S(Q-1) - S(Q+1)]$, and $S(Q) = \sum_{q=1}^{Q}1/q^2$. From this lower bound, we find that more than 90% ICI power is from twelve neighboring subcarriers.

Denote by Ψ_Q the energy of s_k containing in subcarriers $k-Q$ to $k+Q$. A universal lower bound on Ψ_Q/E_s is expressed as [2]

$$\Psi_Q/E_s \geq \min\,\zeta_Q(f),\ \ 0 \leq f \leq 1, \qquad (8)$$

where $\zeta_Q(f) = \pi^{-2}\sin^2(\pi f_d T_s f)\left[(f_d T_s f)^{-2} + \sum_{q=1}^{Q}(f_d T_s f + q)^{-2} + (f_d T_s f - q)^{-2}\right]$. From this lower bound, we can find that when $f_d T_s = 0.1$, more than 98% of the s_k's energy is distributed on the kth subcarrier and two neighboring subcarriers. If $f_d T_s = 0.9$, more than 95% of the symbol energy is contained in nine subcarriers.

In the next subsections, based on the fact that most of a symbol's energy is distributed to a few subcarriers, and the ICI on a subcarrier mainly comes from several neighboring subcarriers, we will develop low-complexity MMSE and DFE receivers.

3.2 Low Complexity MMSE Receiver

Suppose we are interested in detecting symbol s_k. Let $K = 2Q + 1$, and define a $K \times 1$ vector $\boldsymbol{\rho}_k(i) := (k - Q - 1 + i) \bmod N + 1$, $i = 1, \ldots, K$. Let $\mathbf{y}_k = \mathbf{y}(\boldsymbol{\rho}_k)$, $\mathbf{A}_k = \mathbf{A}(\boldsymbol{\rho}_k, :)$, and $\tilde{\mathbf{w}}_k = \tilde{\mathbf{w}}(\boldsymbol{\rho}_k)$. From (3), we have

$$\mathbf{y}_k = \mathbf{A}_k \mathbf{s} + \tilde{\mathbf{w}}_k. \tag{9}$$

The MMSE receiver based on (9) is $\mathbf{m}_k = \mathbf{R}_k^{-1}\mathbf{p}_k$, where $\mathbf{R}_k = E[\,\mathbf{y}_k \mathbf{y}_k^{\mathcal{H}}\,] = E_s \mathbf{A}_k \mathbf{A}_k^{\mathcal{H}} + N_0 \mathbf{I}_K$, and $\mathbf{p}_k = \mathbf{A}_k(:, k)$. The parameter K can be chosen to tradeoff performance for complexity. To detect N symbols, we should find N MMSE receivers $\mathbf{m}_k$, $k \in [0, N-1]$. The major computation on the MMSE receiver is to calculate the covariance matrix $\mathbf{R}_k$ and its inverse. Since the first $K-1$ rows of $\mathbf{R}_{k+1}$ are the same as the last $K-1$ rows of $\mathbf{R}_k$, we can recursively calculate the inverse of $\mathbf{R}_k$, which greatly reduces the computation.

If we partition $\mathbf{A}_k$ into $\mathbf{A}_k = [\mathbf{a}_k \;\; \bar{\mathbf{A}}_k^{\mathcal{H}}]^{\mathcal{H}}$, $\mathbf{R}_k$ can be written as

$$\mathbf{R}_k = \begin{bmatrix} \theta_k & \boldsymbol{\theta}_k^{\mathcal{H}} \\ \boldsymbol{\theta}_k & \boldsymbol{\Theta}_k \end{bmatrix}, \tag{10}$$

where $\theta_k = E_s \mathbf{a}_k^{\mathcal{H}} \mathbf{a}_k + N_0$, $\boldsymbol{\theta}_k = E_s \bar{\mathbf{A}}_k \mathbf{a}_k$, and $\boldsymbol{\Theta}_k = E_s \bar{\mathbf{A}}_k \bar{\mathbf{A}}_k^{\mathcal{H}} + N_0 \mathbf{I}_{K-1}$. Let the inverse of $\mathbf{R}_k$ be

$$\mathbf{R}_k^{-1} = \begin{bmatrix} v_{k,11} & \mathbf{v}_{k,21}^{\mathcal{H}} \\ \mathbf{v}_{k,21} & \mathbf{V}_{k,22} \end{bmatrix}, \tag{11}$$

where $v_{k,11}$ is a scalar, $\mathbf{v}_{k,12}$ is a $(K-1) \times 1$ vector, and $\mathbf{V}_{k,22}$ is a $(K-1) \times (K-1)$ matrix. In [2], we show that

$$\boldsymbol{\Theta}_k^{-1} = \mathbf{V}_{k,22} - \mathbf{v}_{k,21}\mathbf{v}_{k,21}^{\mathcal{H}} / v_{k,11}. \tag{12}$$

If we partition $\mathbf{A}_{k+1}$ into $\mathbf{A}_{k+1} = [\bar{\mathbf{A}}_k^{\mathcal{H}} \;\; \tilde{\mathbf{a}}_{k+1}]^{\mathcal{H}}$, we have

$$\mathbf{R}_{k+1} = \begin{bmatrix} \boldsymbol{\Theta}_k & \tilde{\boldsymbol{\theta}}_{k+1} \\ \tilde{\boldsymbol{\theta}}_{k+1}^{\mathcal{H}} & \tilde{\theta}_{k+1} \end{bmatrix}, \tag{13}$$

where $\tilde{\theta}_{k+1} = E_s \tilde{\mathbf{a}}_{k+1}^{\mathcal{H}} \tilde{\mathbf{a}}_{k+1} + N_0$, $\tilde{\boldsymbol{\theta}}_{k+1} = E_s \bar{\mathbf{A}}_k \tilde{\mathbf{a}}_{k+1}$. Let $\beta_{k+1} = (\tilde{\theta}_{k+1} - \tilde{\boldsymbol{\theta}}_{k+1}^{\mathcal{H}} \boldsymbol{\Theta}_k^{-1} \tilde{\boldsymbol{\theta}}_{k+1})^{-1}$, $\mathbf{b}_{k+1} = -\boldsymbol{\Theta}_k^{-1} \tilde{\boldsymbol{\theta}}_{k+1}$. In [2], we prove that

$$\mathbf{R}_{k+1}^{-1} = \begin{bmatrix} \boldsymbol{\Theta}_k^{-1} + \mathbf{b}_{k+1}\mathbf{b}_{k+1}^{\mathcal{H}}\beta_{k+1} & \mathbf{b}_{k+1}\beta_{k+1} \\ \mathbf{b}_{k+1}^{\mathcal{H}}\beta_{k+1} & \beta_{k+1} \end{bmatrix}. \tag{14}$$

Hence, $\mathbf{R}_{k+1}^{-1}$ can be computed from $\mathbf{R}_k^{-1}$ through $\boldsymbol{\Theta}_k^{-1}$.

Calculating $\boldsymbol{\Theta}_k^{-1}$, $\mathbf{b}_{k+1}$, and β_{k+1} requires $\mathcal{O}(K^2)$, $\mathcal{O}(K^2)$, and $\mathcal{O}(K)$ operations, respectively; the computation of $\tilde{\theta}_{k+1}$ is $\mathcal{O}(N)$, and $\tilde{\boldsymbol{\theta}}_{k+1}$ is $\mathcal{O}(NK)$. Hence, the major computation to obtain $\mathbf{R}_{k+1}^{-1}$ is in calculating $\tilde{\boldsymbol{\theta}}_{k+1}$. To find $\mathbf{R}_0^{-1}$, we need $\mathcal{O}(NK^2)$ operations to calculate $\mathbf{R}_0$, and $\mathcal{O}(K^3)$ operations to invert $\mathbf{R}_0$. Therefore, the total computational complexity of detecting an OFDM block is $\mathcal{O}(N^2 K)$. On the other hand, using an MMSE receiver based on the whole block in (3) as suggested in [4], requires $\mathcal{O}(N^3)$ operations. Since $K \ll N$, the computational complexity reduces substantially.

In the simulations provided in Section 4, we observe an error floor on BER for the MMSE receiver with small K. To improve the BER performance while retaining the low receiver complexity, we develop a DFE receiver in the next subsection.

3.3 Decision Feedback ICI Cancellation

We first find the symbol with the largest energy by ordering the norm of the columns of $\mathbf{A}$. Suppose that s_m has the largest symbol energy. Starting from the mth subcarrier, we detect symbols consecutively, either in the forward order or in the backward order. Suppose we detect symbols in the forward order, then the detection order is $s_m, \ldots, s_{N-1}, s_0, \ldots, s_{m-1}$. We use an MMSE receiver based on the signal vector $\mathbf{y}_m$ given in (9) to detect the symbol s_m. For detecting symbol s_k, $k \neq m$, we reconstruct the signal vectors of the previously detected symbols, and then subtract them from the received signal vector $\mathbf{y}_k$. Letting $\hat{s}_m$ denote the detected symbol of s_m, and $\boldsymbol{\varrho}(i) := (m + i - 1) \bmod N$, $i = 1, \ldots, N$, we have $\tilde{\mathbf{y}}_k = \mathbf{y}_k - \sum_{i=1}^{n_k} A_k(:, \boldsymbol{\varrho}(i)+1)\hat{s}_{\boldsymbol{\varrho}(i)}$, where $k = \boldsymbol{\varrho}(2), \boldsymbol{\varrho}(3), \ldots, \boldsymbol{\varrho}(N)$, $n_k = k - m$, $k > m$, or $n_k = N - m + k$, $k < m$. Assume that all previous symbols are detected correctly, i.e., $\hat{s}_{\boldsymbol{\varrho}(i)} = s_{\boldsymbol{\varrho}(i)}$, $i \in [1, n_k]$, $\tilde{\mathbf{y}}_k$ is found from (9) as $\tilde{\mathbf{y}}_k = \tilde{\mathbf{A}}_k \tilde{\mathbf{s}}_k + \tilde{\mathbf{w}}_k$, where $\tilde{\mathbf{A}}_k = \mathbf{A}_k(:, \boldsymbol{\varrho}(n_k + 1 : N) + 1)$, and $\tilde{\mathbf{s}}_k = \mathbf{s}(\boldsymbol{\varrho}(n_k + 1 : N) + 1)$. If we also rearrange the columns of $\mathbf{A}_m$ to obtain $\tilde{\mathbf{A}}_m = \mathbf{A}_m(:, \boldsymbol{\varrho} + 1)$, the first $K-1$ rows of $\tilde{\mathbf{A}}_{k+1}$ are the same as the last $K-1$ rows of $\tilde{\mathbf{A}}_k$, except that the first column of $\tilde{\mathbf{A}}_k$ is removed. Based on this fact, we can modify the recursive method in the last subsection to find the MMSE DFE receiver for s_k.

We partition the matrix $\tilde{\mathbf{A}}_k$ in the same manner as partitioning $\mathbf{A}_k$. With slightly misusing notation, we still denote the covariance matrix of $\tilde{\mathbf{y}}_k$ as $\mathbf{R}_k$ which is partitioned in (10). Now, we write $\tilde{\mathbf{A}}_{k+1}$ as $\tilde{\mathbf{A}}_{k+1} = [\mathbf{B}_{k+1}^{\mathcal{H}} \;\; \tilde{\mathbf{a}}_{k+1}]^{\mathcal{H}}$, where $\mathbf{B}_{k+1} = \tilde{\mathbf{A}}_k(:, 2 : N - n_k)$. Note that the $(K-1) \times (N - n_k - 1)$ matrix $\mathbf{B}_{k+1}$ contains the last $N - n_k - 1$ columns of the $(K-1) \times (N - n_k)$ matrix $\bar{\mathbf{A}}_k$. The covariance matrix of $\tilde{\mathbf{y}}_{k+1}$, $\mathbf{R}_{k+1}$, is expressed as

$$\mathbf{R}_{k+1} = \begin{bmatrix} \tilde{\boldsymbol{\Theta}}_{k+1} & \tilde{\boldsymbol{\theta}}_{k+1} \\ \tilde{\boldsymbol{\theta}}_{k+1}^{\mathcal{H}} & \tilde{\theta}_{k+1} \end{bmatrix}, \tag{15}$$

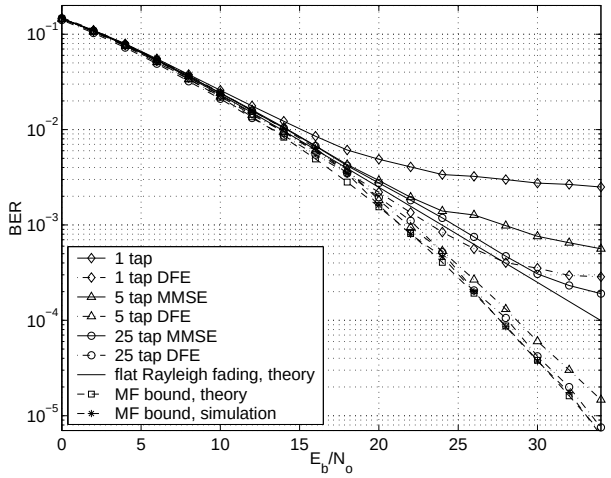

Figure 1: BER comparison, perfect CSI, $f_dT_s = 0.05$

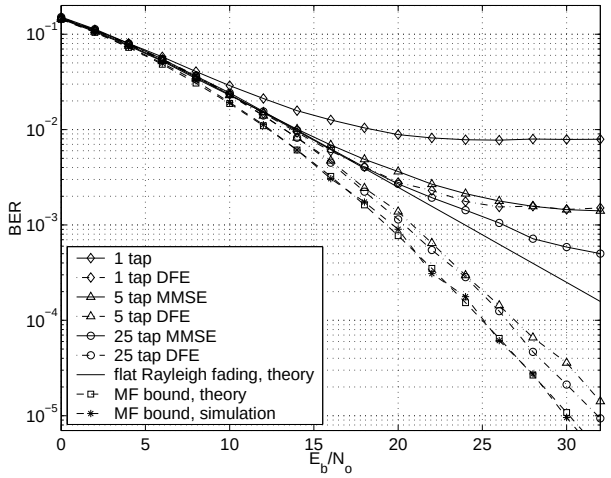

Figure 2: BER comparison, perfect CSI, $f_dT_s = 0.1$

where $\tilde{\mathbf{\Theta}}_{k+1} = E_s\mathbf{B}_{k+1}\mathbf{B}_{k+1}^{\mathcal{H}} + N_0\mathbf{I}_{K-1}$, $\tilde{\theta}_{k+1} = E_s\tilde{\mathbf{a}}_{k+1}^{\mathcal{H}}\tilde{\mathbf{a}}_{k+1} + N_0$, $\tilde{\boldsymbol{\theta}}_{k+1} = E_s\mathbf{B}_{k+1}\tilde{\mathbf{a}}_{k+1}$. Letting $\boldsymbol{\alpha}_k = \bar{\mathbf{A}}_k(:,1)$, we have $\tilde{\mathbf{\Theta}}_{k+1} = \mathbf{\Theta}_k - E_s\boldsymbol{\alpha}_k\boldsymbol{\alpha}_k^{\mathcal{H}}$. The inverse of $\tilde{\mathbf{\Theta}}_{k+1}$ can be found using the matrix inversion lemma [5, p. 19] as $\tilde{\mathbf{\Theta}}_{k+1}^{-1} = \mathbf{\Theta}_k^{-1} + (\mathbf{\Theta}_k^{-1}\boldsymbol{\alpha}_k)(\mathbf{\Theta}_k^{-1}\boldsymbol{\alpha}_k)^{\mathcal{H}}/(E_s^{-1} - \boldsymbol{\alpha}_k^{\mathcal{H}}\mathbf{\Theta}_k^{-1}\boldsymbol{\alpha}_k)$. Let $\beta_{k+1} = (\tilde{\theta}_{k+1} - \tilde{\boldsymbol{\theta}}_{k+1}^{\mathcal{H}}\tilde{\mathbf{\Theta}}_{k+1}^{-1}\tilde{\boldsymbol{\theta}}_{k+1})^{-1}$, $\mathbf{b}_{k+1} = -\tilde{\mathbf{\Theta}}_{k+1}^{-1}\tilde{\boldsymbol{\theta}}_{k+1}$, then, $\mathbf{R}_{k+1}^{-1}$ can be computed from (14) by replacing $\mathbf{\Theta}_k^{-1}$ with $\tilde{\mathbf{\Theta}}_{k+1}^{-1}$. The major computation to find $\mathbf{R}_{k+1}^{-1}$ is on calculating $\tilde{\boldsymbol{\theta}}_{k+1}$, which requires $\mathcal{O}((K-1)(N-n_k))$, where $k = \boldsymbol{\varrho}(n_k)$ and $n_k = 1, \ldots, N-1$. Since $\sum_{n=1}^{N} n = N(N-1)/2$, the complexity of the DFE receiver is $\mathcal{O}(N^2K)$, which is in the same order as that of the MMSE receiver.

After the MMSE DFE receiver makes tentative decisions on N symbols, we can use parallel interference cancellation (PIC) to improve the BER performance. Specifically, let $\hat{\mathbf{y}}_k = \mathbf{y}_k - \sum_{\substack{m=0 \\ m\neq k}}^{N-1} \mathbf{A}_k(:, m+1)\hat{s}_m$, then the decision variable for s_k is $z_k = \mathbf{A}_k^{\mathcal{H}}(:, k+1)\hat{\mathbf{y}}_k$. This PIC procedure may run more than one iteration to enhance the BER performance. Each PIC iteration requires $\mathcal{O}(N^2)$ operations, which does not increase the computation significantly.

3.4 Channel Estimation

The MMSE and DFE receivers require channel state information (CSI). If we use pilot tones to estimate the time varying channel, the channel estimator itself suffers from ICI. Here, we multiplex pilot symbols with the OFDM blocks in the time domain, as proposed in [4]. If we insert a pilot symbol block of length T_{ps} in every N_{ps} OFDM block, then we should choose N_{ps} and T_{ps} so that $N_{ps}T_b + T_{ps} < 1/(2f_d)$ [3]. On the other hand, once N_{ps} and T_{ps} have been selected, the normalized Doppler frequency should be $f_dT_s < T_s/[2(N_{ps}T_b + T_{ps})]$. If the system is required to operate when $f_dT_s \geq T_s/[2(N_{ps}T_b + T_{ps})]$ we need to consider alternative channel estimation scheme; or, we should jointly design the transmitter and receiver to collect the temporal diversity without suffering from the interference.

4 Simulations

In his section, we test the MMSE and DFE ICI suppression schemes via computer simulations. The number of the subcarriers is chosen to be $N = 128$, and the length of the cyclic prefix is $N_p = N/8$. The QPSK constellation is adopted, and the bit energy is $E_b = E_s/2$. We use a 2-tap fading channel with an exponential delay power spectrum, i.e., $\sigma_l^2 = \exp(-l/L)/\sum_{l=0}^{L-1}\sigma_l^2$, $L = 2$, and $l = 0, 1$. Each channel tap is a complex Gaussian random process independently generated with the classical Doppler spectrum based on the Jakes' model [6]. The delay of the first tap is zero, and the delay of the second tap is generated from the set $\{T_c, 2T_c, \ldots, N_pT_c\}$ with equal probability. In the DFE detection, we use two iterations. *Test Case 2 (perfect CSI):* Figs. 1, 2, and 3 compare the BER performance of the MMSE and DFE equalizers for different Doppler frequencies. The theoretical BER for the flat Rayleigh fading channel, the theoretical MFB calculated from (4), and the simulated MFB are also displayed in these figures. From the MFB, we see that the time variations of the channel introduce the temporal diversity which increases as the Doppler frequency becomes large. While the BER performance of the MMSE equalizer improves as the number of the equalizer taps K increases, it still exhibits an error floor at high E_b/N_0. The DFE equalizer outperforms the MMSE equalizer with the same number of taps. However, the 1-tap DFE still has poor performance even when the Doppler frequency is as low as $f_dT_s = 0.05$. The 5-tap DFE equalizer has significant performance improvement over the 1-tap DFE equalizer, and its BER curve is close to that of the 25-tap equalizer. The small gap between the MFB and the

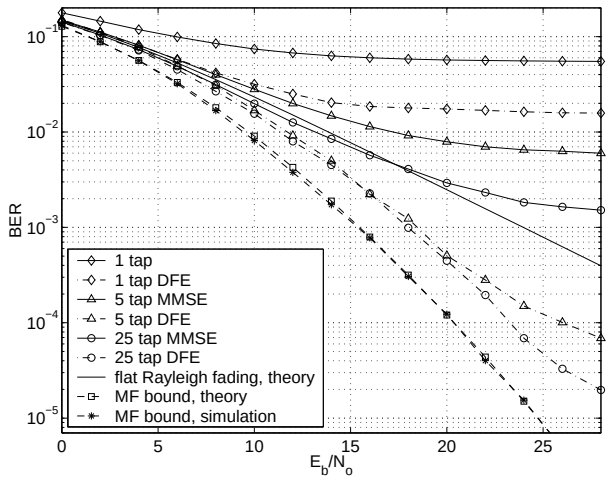

Figure 3: BER comparison, perfect CSI, $f_dT_s = 0.3$

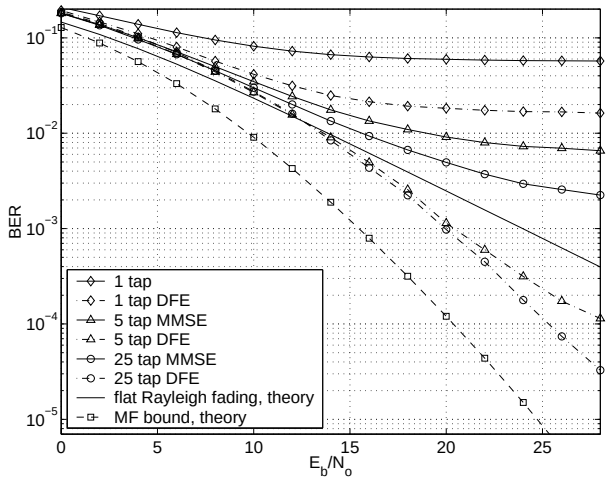

Figure 4: BER comparison, estimated CSI, $f_dT_s = 0.3$

BER of 5-tap DFE equalizer shows that we can suppress ICI effectively and improve the BER performance significantly with a low-complexity DFE equalizer.

Test Case 2 (estimated CSI): In this test, the channel is estimated using the pilot symbols, and the BER is shown in Fig. 4 with $f_dT_s = 0.3$. To ensure that the rate of the pilot blocks is higher than $f_d/2$, every OFDM block is followed by a pilot block of length $2T_p$. A 10-tap MMSE filter is used to estimate the channel [3]. If we compare the BER curves displayed in Fig. 4 and Fig. 3, we see that the channel estimation error results in slight BER degradation.

5 Conclusions

We derived an MFB for OFDM in doubly-selective fading channels, and showed that the channel variations introduce temporal diversity, which has the potential to improve the BER performance if properly exploited. We also studied the ICI and energy leakage that are caused by the time varying channel. Our universal bounds showed that the most of the symbol energy is distributed on a few subcarriers, and the ICI power over a subcarrier mainly comes from several neighboring subcarriers. Based on these facts, we developed low-complexity MMSE and DFE receivers. While the low-complexity MMSE receiver exhibits an error floor, the DFE receiver can collect the temporal diversity, and its BER performance comes close to the MFB at relatively low f_dT_s.

References

[1] J. Armstrong, "Analysis of new and existing methods of reducing intercarrier interference due to carrier frequency offset in OFDM," *IEEE Trans. Commun.*, vol. 47, pp. 365–369, Mar. 1999.

[2] X. Cai and G. B. Giannakis, "Bounding performance and suppressing inter-carrier interference in wireless mobile OFDM," *IEEE Trans. Commun.*, submitted, July 2002.

[3] J. K. Cavers, "An analysis of pilot symbol assisted modulation for Rayleigh fading channels," *IEEE Trans. Veh. Technol.*, vol. 40, pp. 686–693, Nov. 1991.

[4] Y.-S. Choi, P. J. Voltz, and F. A. Cassara, "On channel estimation and detection for multicarrier signals in fast and selective Rayleigh fading channels," *IEEE Trans. Commun,*, vol. 49, pp. 1375–1387, Aug. 2001.

[5] R. A. Horn and C. R. Johnson, *Matrix Analysis*. New York: Cambridge University Press, 1985.

[6] W. C. Jakes, *Microwave Mobile Communications*. New York: Wiley, 1974.

[7] Y. G. Li and L. J. Cimini, "Bounds on the interchannel interference of OFDM in time-varying impairments," *IEEE Trans. Commun.*, vol. 49, pp. 401–404, Mar. 2001.

[8] F. Ling, "Matched filter-bound for time-discrete multipath Rayleigh fading channels," *IEEE Trans. Commun.*, vol. 43, pp. 710–713, Feb./Mar./Apr. 1995.

[9] J. G. Proakis, *Digital Communications*. McGraw-Hill, 1995.

[10] M. Russell and G. L. S. Stüber, "Interchannel interference analysis of OFDM in a mobile environment," in *Proc. of VTC'95*, Chicago, Illinois, pp. 820–824, July 1995.

[11] F. Sanzi and J. Speidel, "An adaptive two-dimensional channel estimation for wireless OFDM with application to mobile DVB-T," *IEEE Trans. Broadcasting*, vol. 46, pp. 128–133, June 2000.

[12] Y. Zhao and S. Häggman, "Intercarrier interference self-cancellation scheme for OFDM mobile communication systems," *IEEE Trans. Commun.*, vol. 49, pp. 1185–1191, July 2001.